Astrocyte pVHL and HIF-α isoforms are required for embryonic-to-adult vascular transition in the eye

Toshihide Kurihara,[1] Peter D. Westenskow,[1] Tim U. Krohne,[1] Edith Aguilar,[1] Randall S. Johnson,[2] and Martin Friedlander[1]

[1]Department of Cell Biology, The Scripps Research Institute, La Jolla, CA 92037
[2]Molecular Biology Section, Division of Biological Sciences, University of California San Diego, La Jolla, CA 92093

Successful transition from embryonic to adult circulation is critical for survival of mammalian organisms. This shift occurs in the central cardiovascular circulation and in the eye as oxygen tension increases. However, its regulation is not well understood. We have used combinatorial gene deletion and overexpression assays to assess the effect of astrocyte-targeted deletion of von Hippel–Lindau tumor suppressor (*Vhl*), hypoxia-inducible factor-αs (*Hif-αs*), and *Vegf* on the normal regression of the hyaloidal vessels, the fetal ocular circulation system. Astrocytic *Vhl* deletion induced accelerated hyaloidal regression and subsequent massive secondary outgrowth. Combinatorial gene deletion involving *Vhl*, *Hif-αs*, and *Vegf* genes revealed that HIF-2α/vascular endothelial growth factor signaling induces secondary outgrowth in *Vhl* mutants. Conversely, HIF-1α regulated macrophage migration inhibitory factor and promoted macrophage infiltration that accelerates hyaloidal vessel regression. The phenotype observed in *Vhl* mutants strongly resembles human persistent hyperplastic primary vitreous cases and may provide insights into vascular remodeling mechanisms in other systems.

Introduction

Dynamic changes in oxygen demand can induce systemic alterations to the vasculature of organisms during development. In the embryonic eye, oxygen is delivered to ocular tissues through the hyaloidal vasculature, a transient network that is established during early optic cup stages and is important for the development of the lens, vitreous, and retina. The hyaloidal vasculature consists of different distinct anatomical structures, including the hyaloidal artery (HA), the vasa hyaloidea propria, and the tunica vasculosa lentis (Fig. 1 A). By the third trimester in humans and in postnatal 3–4-wk-old rodents, the hyaloidal network undergoes apoptosis and regresses (Ito and Yoshioka, 1999; Brown et al., 2005). Starting at birth and continuing through the first postnatal month, the neurosensory retina matures, and the adult retinal vasculature develops as three distinct vascular plexuses, each localized to a specific plane in the retina. The inner plexus appears first and is localized to the inner retina ganglion cell layer. The outer plexus forms at the outer edge of the inner nuclear layer, and, finally, an intermediate vascular plexus is formed at the inner edge of the inner nuclear layer. Importantly, the formation and maturation of the retinal vasculature occur concomitant with hyaloidal vessel regression in both humans and rodents, suggesting that the two processes may be intrinsically linked and regulated by oxygen availability (Fig. 1 B; Ye et al., 2009; Kurihara et al., 2010).

The precise mechanisms controlling hyaloidal vessel regression are not clear, but if the vessels do not completely regress in humans, persistent hyperplastic primary vitreous (PHPV; Reese, 1955; Goldberg, 1997) may occur and cause blindness in neonates. Several nonexclusive hypotheses of the vascular abnormalities observed in PHPV have been proposed, including the cessation of hyaloidal vascular blood flow (Lang et al., 1994; Meeson et al., 1996; Brown et al., 2005), accumulation of antiangiogenic factors pooling in the vitreous (Preis et al., 1977; Lutty et al., 1983), or the production of cytokines from infiltrating macrophages that induce apoptosis in the endothelial cells (Lang and Bishop, 1993; Lang et al., 1994; Diez-Roux and Lang, 1997; Lobov et al., 2005; Albè et al., 2008).

T. Kurihara and P.D. Westenskow contributed equally to this paper.

Correspondence to Martin Friedlander: friedlan@scripps.edu

Abbreviations used in this paper: CSLO, confocal-scanning laser ophthalmoscopy; GFAP, glial fibrillary acidic protein; HA, hyaloidal artery; HIF, hypoxia-inducible factor; ICG, indocyanine green; LysM, M lysozyme; MIF, macrophage migration inhibitory factor; OCT, optical coherence tomography; PHPV, persistent hyperplastic primary vitreous; pVHL, VHL protein; rmMIF, recombinant murine MIF; VHL, von Hippel–Lindau.

The Rockefeller University Press $30.00
J. Cell Biol. Vol. 195 No. 4 689–701
www.jcb.org/cgi/doi/10.1083/jcb.201107029

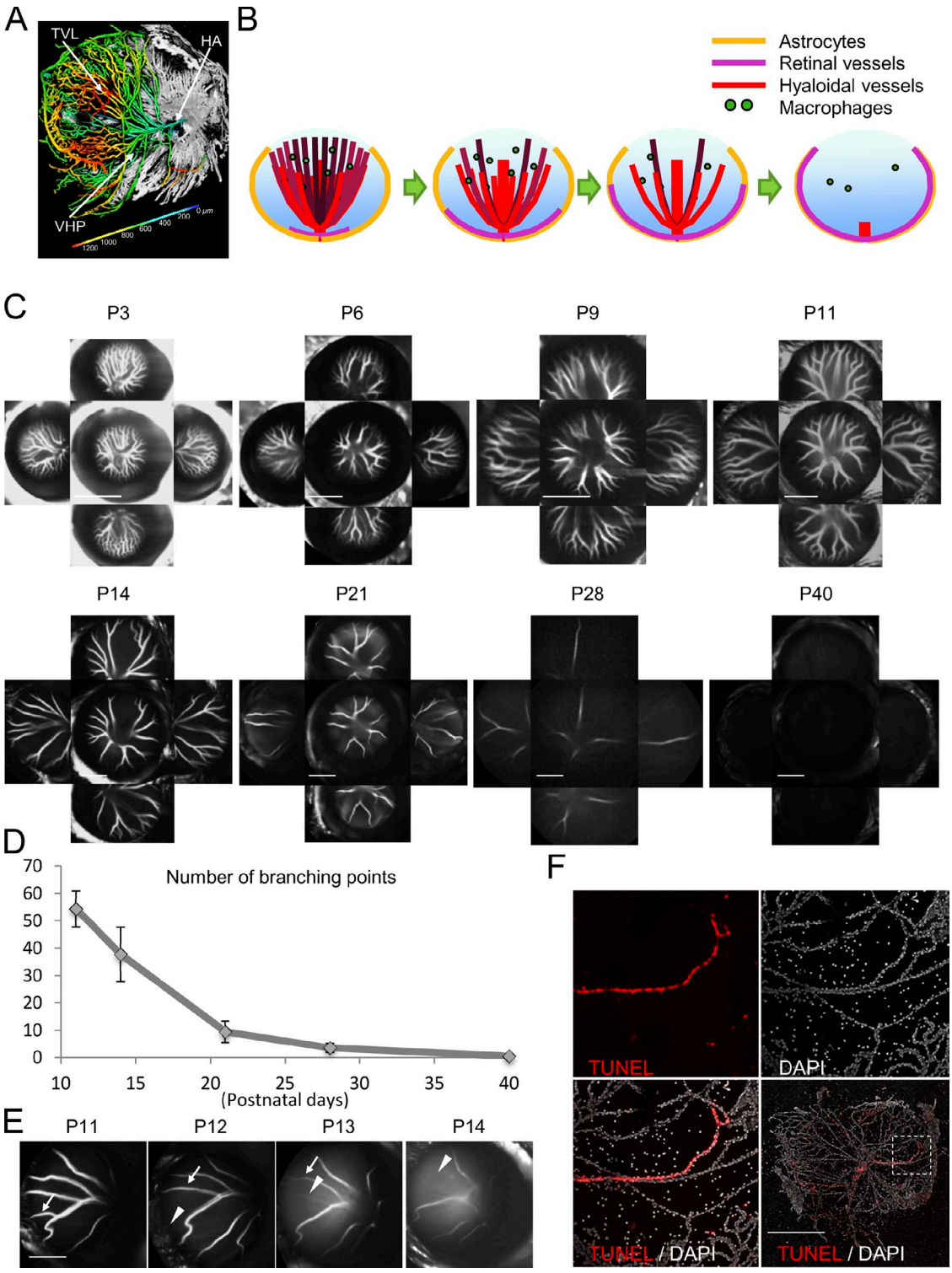

Figure 1. **Development of in vivo hyaloidal vascular apoptosis assay system.** (A) Vascular cast of a wild-type C57BL/6j P9 eye. Hyaloidal vasculature is colored according to the depth from the optic nerve head. TVL, tunica vasculosa lentis; VHP, vasa hyaloidea propria. (B) Schematic hyaloidal regression model. Note that the formation and maturation of the retinal vasculature on the astrocytes occur concomitant with hyaloidal vessel regression. (C and D) The progression and dynamics of hyaloidal vessel regression monitored in vivo using CSLO and ICG angiography. (C) Representative images of the regressing hyaloidal network from five different angles show central and peripheral vessels at various developmental stages in wild-type C57BL/6j mice. (D) Regression is quantified by counting the number of branching points of vessels derived from the central vessels. Values from key time points in hyaloidal vascular regression are plotted on a scatter plot as the number of branching points (y axis) at P11, 14, 21, 28, and 40 developmental stages (x axis; n = 6–8). Note that hyaloidal vessels are abundant and extensively branched at early stages but mostly absent by P40. Error bars indicate mean ± SD. (E) The daily regression of single vessels is shown over a 4-d span in a live animal. Arrows in each panel mark a vessel that is regressing; arrowheads label the space that the vessel occupied over the previous days. (F) TUNEL staining (top left) and DAPI counterstaining (top right) of the P6 hyaloidal network (merged in bottom left and right; marked by boxed area) marks entire vessels. Note that hyaloidal vascular regression visualized by in vivo imaging follows endothelial apoptosis. Bars: (C and E) 2,000 µm; (F) 1,000 µm.

Alternatively, mutations to the Arf tumor suppressor ($p19^{Arf}$) or downstream effector protein p53 may induce hyaloidal vessel persistence (McKeller et al., 2002). This is significant and may be relevant to PHPV because p53 functions as a tumor suppressor by inducing apoptosis in response to stress, including hypoxia (Messmer-Blust et al., 2009). Additionally, Wnt/β-catenin signaling has been shown to regulate hyaloidal vessel regression; Wnt7b released from macrophages associates with Frz4/Lrp5 receptors and activates the canonical Wnt pathway to induce programmed cell death in hyaloidal endothelial cells (Kato et al., 2002; Xu et al., 2004; Lobov et al., 2005; Ye et al., 2009). In humans, mutations to Wnt7b, Frz4, or Lrp5 have been linked to familial exudative vitreoretinopathy and Norrie disease with PHPV. However, most cases of PHPV are unilateral and not linked to any specific genetic mutations (Reese, 1955; Goldberg, 1997). Hence, it is important to better understand mechanisms underlying the normal regression of the hyaloidal vasculature as well as those factors that contribute to abnormalities in this process.

During normoxia, von Hippel–Lindau protein (pVHL), a substrate recognition component of an E3-ubiquitin ligase, efficiently and rapidly destabilizes hypoxia-inducible factor (HIF) α subunits (e.g., HIF-1α and HIF-2α). During hypoxia, HIF-αs accumulate, translocate to the nucleus, and regulate the expression of HIF target genes that control diverse cellular processes such as glycolytic metabolism, cell proliferation, and angiogenesis (Maxwell et al., 1999). A requirement for HIF-1α regulation of hyaloidal regression has been demonstrated in transgenic mice. We have previously demonstrated persistence of hyaloidal vasculature after conditional inactivation of pVHL and resulting HIF hyperactivity in sensory retinal cells; furthermore, the vascular defects in these mice were rescued by deleting *Hif-1α* or through local VEGF inhibition (Kurihara et al., 2010). Persistent hyaloidal vasculature is also observed in *Cbp/p300-interacting transactivator with Glu/Asp-rich carboxy-terminal domain 2 (Cited2*$^{-/-}$*)* mice (Chen et al., 2008). Cited2 is expressed in the embryonic lens and is a negative transcriptional modulator of HIF-1α. The conditional deletion of *Hif-1α* in the lens of *Cited2*$^{-/-}$ mice rescues the vascular phenotype by limiting VEGF expression. Therefore, in the retina and lens, the oxygen-sensitive HIF-1α proteins function to promote angiogenesis of the hyaloidal vasculature.

Retinal astrocytes colocalize with the inner layer of retinal blood vessels on the vitreal surface of the retina, making them ideal oxygen sensors during the neonatal period, during which the most dramatic vascular changes (e.g., hyaloidal regression and retinal vascular development) are occurring. In this study, we perform genetic gain- and loss-of-function assays of the pVHL/HIF signaling pathway in astrocytes. We also perform transplantation assays with astrocytes ectopically expressing dominant-stable *Hif-1α* and *Hif-2α* genes to mimic a hypoxic response. Using these techniques, we show that HIF-1α and HIF-2α exert divergent regulatory functions during hyaloidal vessel regression. We present a model that may serve to alter prevailing concepts of how PHPV in humans progresses, thereby helping to develop more effective therapeutic interventions. In addition, we suggest that this work may serve as a model for macrophage-mediated vascular remodeling in other systems.

Results

Regression of the hyaloidal vasculature can be effectively monitored in vivo

Components of the hyaloidal vasculature including HA, vasa hyaloidea propria, and tunica vasculosa lentis in the vitreous cavity are the primary blood supply for the eye during embryonic and early postnatal stages (Fig. 1 A). Previous studies have examined hyaloidal regression using sectioned or isolated hyaloidal vasculature (Ito and Yoshioka, 1999; Kato et al., 2002; McKeller et al., 2002; Lobov et al., 2005). However, these techniques do not permit adequate visualization of the vascular network; vessels are fragile and may be lost during dissection, and their 3D relationships to each other and the posterior segment of the eye are not adequately visualized. Therefore, we established a novel in vivo imaging technique that combines confocal-scanning laser ophthalmoscopy (CSLO) and indocyanine green (ICG) angiography. Using this system, we systematically monitored the regression of the hyaloidal vasculature across several developmental stages in vivo (Fig. 1 C). The number of branching points of the vessels was also counted from these images to quantify the rate of regression (Figs. 1 D and S1). By postnatal day 28 (P28), the number of branching points of hyaloidal vessels was minimal, and few vessels were detectable by P40 (Fig. 1, C and D). These findings were consistent with data obtained from a previous study (Ito and Yoshioka, 1999), thus validating the use of this technique to monitor hyaloidal regression. By using this in vivo imaging technique, the dynamics of hyaloidal regression can be monitored in real time, and rodents do not have to be sacrificed at each time point, thus maximizing the information obtained from each individual. In fact, we were able to monitor the loss of individual vessels over a 4-d span (Fig. 1 E). TUNEL positivity of intact vessels is also observed in stage P6 isolated hyaloidal vasculature (Fig. 1 F), implying that the apoptotic stimulus once received may be passed quickly through endothelial cells in intact vessels. Collectively, these results demonstrate that in vivo CSLO and ICG angiography is an excellent system for examining the progression of hyaloidal regression.

Conditional deletion of *Vhl* in astrocytes results in accelerated primary hyaloidal vascular regression followed by massive secondary neovascularization

We previously reported persistent hyaloidal vasculature in postnatal mouse eyes after conditional *Vhl* deletion in neural retinal cells (Kurihara et al., 2010). Because of their colocalization with retinal vessels (but not with the hyaloidal vasculature; Fig. S2) and known roles in angiogenesis, we hypothesized that pVHL/HIF signaling in astrocytes may also play a critical role in hyaloidal vascular regression. To determine the function of pVHL in hyaloidal vessel regression, we used a conditional deletion approach to inactivate *Vhl* using floxed alleles in *glial fibrillary acidic protein* (*GFAP*)–*Cre* mice (Fig. S3; Bajenaru et al., 2002). In these mice, recombination occurs in retinal astrocytes during neonatal stages (Weidemann et al., 2009, 2010).

Using CSLO, we serially imaged the hyaloidal vessels from their entrance into the eye at the optic nerve to their terminal tips on the posterior lens. We confirmed that the primary hyaloidal vascular stalk emerged from the optic nerve head and branched as it crossed the posterior vitreous cavity during the early postnatal period (Fig. 2 A). In control mice, the vessels branch frequently as they follow convoluted paths through the vitreous toward the peripheral regions of the lens (Fig. 2 A). Between P13 and 18, transgenic mice with *Vhl* mutations had significantly accelerated primary hyaloidal vessel regression compared with littermate controls (P = 0.00066, 0.0098, and 0.011 at P13, 15, and 18, respectively; Fig. 2 B). However, at P20, significantly more branching points of primary hyaloidal vessels were observed in the transgenic mice compared with littermate controls (P = 0.044; Fig. 2 B). Dense aggregates of vessels coalescing around the central HA were observed in deeper layers of the vitreous closer to the optic nerve head (Fig. 2 A). By P23, these aggregates of vessels were observed in the anterior vitreous near the lens, whereas few vessels are observed in littermate controls (Fig. 2 A). These vessels persisted throughout the lives of the animals and were observed as late as P248 (Fig. 2 C), the longest that the transgenic mice were observed to survive. Retinal vascular defects were also observed; the transgenic mice had areas of massively diluted and highly branched vessels, changes that were not observed in littermate controls (Fig. S4; Weidemann et al., 2010). Additionally, an increase of astrocytic density was observed in *Vhl* mutants (Fig. S4). High-resolution CSLO (Fig. 2 D), histological analysis (Fig. 2 E), optical coherence tomography (OCT; Fig. 2 F), and corrosion casts (Fig. 2 G) of the hyaloidal vascular regrowth in transgenic animals demonstrated a clear connection to the ophthalmical artery as it emerged from the optic nerve head. These findings suggest that HA remains viable and can respond to proangiogenic cues during later postnatal stages. These data also clearly demonstrate a strict requirement for pVHL for the regulation of normal hyaloidal vessel regression and prevention of PHPV. Finally, as the terminal features of this phenotype strongly resemble features of human cases of PHPV (Reese, 1955; Goldberg, 1997), the PHPV phenotype in humans may not simply be caused by failure of the primary hyaloidal vasculature to regress but may also be caused by secondary outgrowth of the primary hyaloidal vascular structures.

Conditional deletion strategies reveal divergent functions of *Hif-1α* or *Hif-2α* in retinal astrocytes

To more clearly understand the molecular mechanism of *Vhl* activity in astrocytes, we deleted it in combination with one or both of the downstream targets *Hif-1α* or *Hif-2α*. In adult mice (P40), massive secondary outgrowth was observed in *Vhl/Hif-1α* double mutants but not in *Vhl/Hif-2α* double mutants or *Vhl/Hif-1α/Hif-2α* triple mutants (Fig. 3 A). These findings strongly suggest that the *Hif-2α* gene in astrocytes is primarily responsible for the persistence and outgrowth of the hyaloidal vessels. VEGF is a direct target of HIFs and a well-characterized proangiogenic factor. Therefore, we hypothesized that an increase in *Vegf* expression in the eye, secondary to *Vhl* deletion (Weidemann et al., 2010), might be responsible for inducing the secondary outgrowth. Similar to observations made in *Vhl/Hif-2α* double and *Vhl/Hif-1α/Hif-2α* triple mutants, the secondary outgrowth was not observed in *Vhl/Vegf* double mutants (Fig. 3 A). These data demonstrate that pVHL/HIF-2α/VEGF signaling is responsible for generating the outgrowth phenotype in *Vhl* mutants in late neonatal stages.

To determine the activity of HIFs in astrocytes at different time points and to determine why the vessels initially regress at faster rates in younger *Vhl* mutant mice, we examined the phenotypes of *Vhl* mutants and the double or triple combinational mutants at P14. Significantly accelerated hyaloidal regression was observed in *Vhl*, *Vhl/Hif-1α*, *Vhl/Hif-2α*, or *Vhl/Vegf* double mutants compared with littermate controls but not in *Vhl/Hif-1α/Hif-2α* triple mutants (P = 0.0025, 0.0033, 0.015, and 0.032 for *Vhl*, *Vhl/Hif-1α*, *Vhl/Hif-2α*, and *Vhl/Vegf*, respectively; Fig. 3 B; quantified in Fig. 3, C–G). These findings suggest that HIF-1α and HIF-2α function independently of VEGF to mediate the accelerated regression phenotype.

Collectively, these results suggest that in astrocytes, HIF-1α and HIF-2α may exert differential effects on hyaloidal vessel stability. Although HIF-2α appears to induce later-stage proangiogenic stabilization of the hyaloidal vessels (through VEGF up-regulation; Fig. 3 A), both HIF-1α and HIF-2α may induce events that lead to apoptosis in hyaloidal vessels. These findings are significant, as a role for HIF-1α in astrocytes has not been previously reported (Weidemann et al., 2009, 2010).

HIF-1α in astrocytes regulates macrophage infiltration by regulating expression of macrophage migration inhibitory factor (MIF)

MIF was first identified as a regulator of macrophage infiltration (Bloom and Bennett, 1966) and was shown to be a direct target of HIF-1α in fibroblasts under hypoxic conditions through interaction with a hypoxia response element on its promoter (Welford et al., 2006). Based on this, we decided to analyze the temporal and spatial changes in *Mif* expression in wild-type postnatal developing eyes during hyaloidal regression. Using real-time RT-PCR analyses of homogenized murine retinas, we observed a progressive reduction of *Mif* transcripts from P3 to 14 (at P14, its expression was significantly down-regulated compared with P3 or 9 [P = 0.00025 or 0.043, respectively]) before stabilization (Fig. 4 A). Importantly, this pattern is inversely correlated with known patterns of oxygen concentration in the inner retina (Yu and Cringle, 2001; Kurihara et al., 2010) during hyaloidal regression and retinal vascular development on astrocytes. Using immunohistochemistry, MIF was detected in GFAP-positive retinal astrocytes at multiple time points (P14-staged retina is shown in Fig. 4 B). Importantly, in *Vhl/Hif-2α* double mutants, in which HIF-1α was constitutively activated and hyaloidal regression was accelerated, significantly increased expression of *Mif* mRNA was detected at P14 (P = 0.030; Fig. 4 C). Additionally, *F4/80* (a macrophage-specific marker) expression was also twofold up-regulated (P = 0.043; Fig. 4 C).

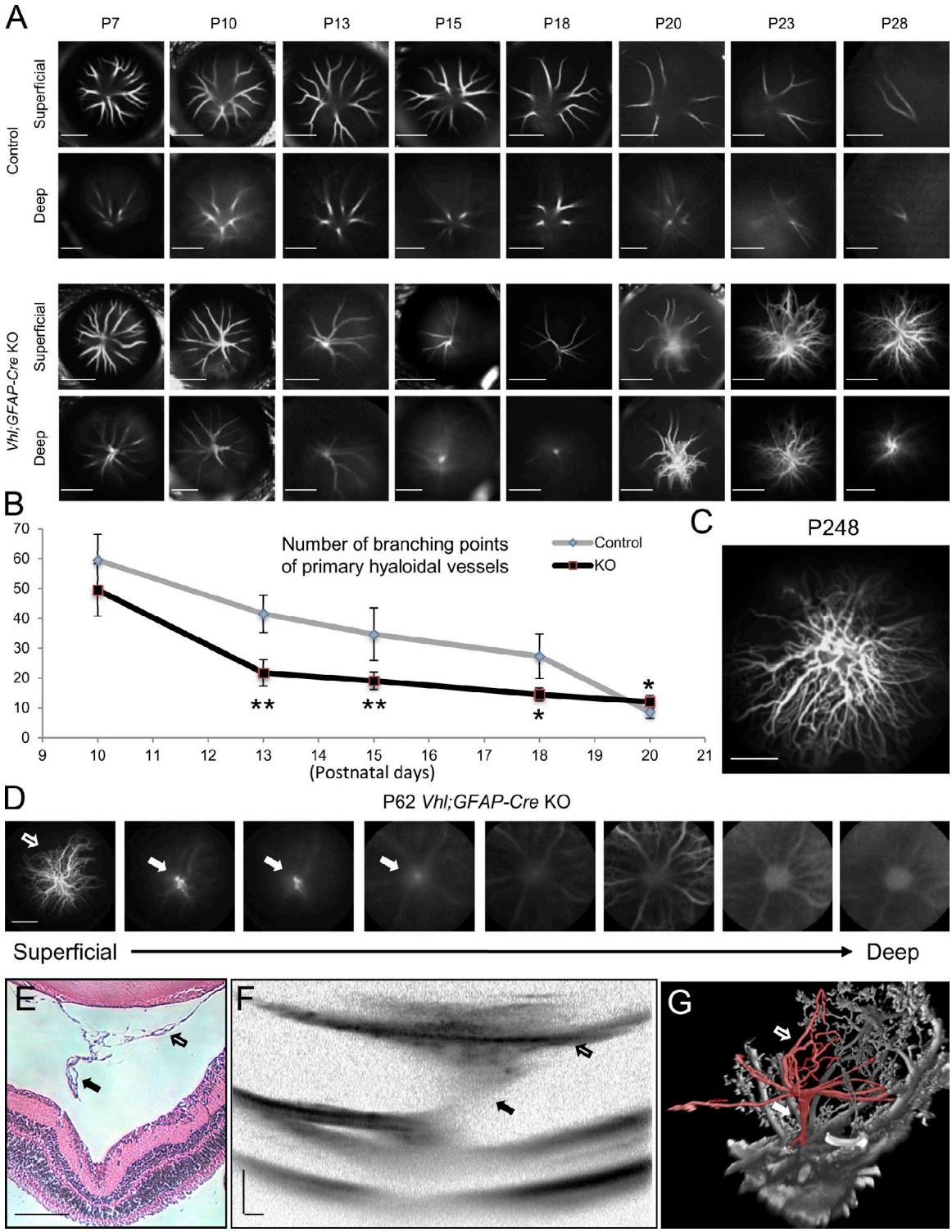

Figure 2. **Development of persistent hyaloidal vasculature in *Vhl;GFAP-Cre* knockout (KO) mice.** (A–C) The conditional deletion of *Vhl* in astrocytes using *GFAP-Cre* induces early accelerated regression of hyaloidal vessels followed by massive secondary outgrowth. (A) Representative in vivo images of hyaloidal vasculature in two different dimensional depth of *Vhl* mutants (third and fourth rows) and control littermates (first and second rows) from P7 to 28. (B) Quantification of the primary (but not secondary outgrowth of) hyaloidal vasculature at P10, 13, 15, 18, and 20 on a scatter plot (n = 4–6). *, $P < 0.05$; **, $P < 0.01$. Error bars indicate mean ± SD. (C) Secondary outgrowth of hyaloidal vasculature observed at stage P248 (~8 mo). Note that vessels form a stalk formation in the deep optical vitreal regions in early stages (fourth row in A). Significantly fewer branching point numbers of the primary hyaloidal vasculature were observed in *Vhl* mutants compared with controls during P13 to 18 stages (B). Pronounced secondary outgrowth from the stalk occurs from P20 and persists throughout the lives of the *Vhl* mutants (A and C). (D–G) Stalk formation observed in CSLO (D), paraffin-embedded section (E), OCT (F), and in vascular casts (G). Note the connecting stalk (closed arrows) between the secondary outgrowth (open arrows) and the optic artery. Bars: (A, C, and D) 2,000 µm; (E and F) 200 µm.

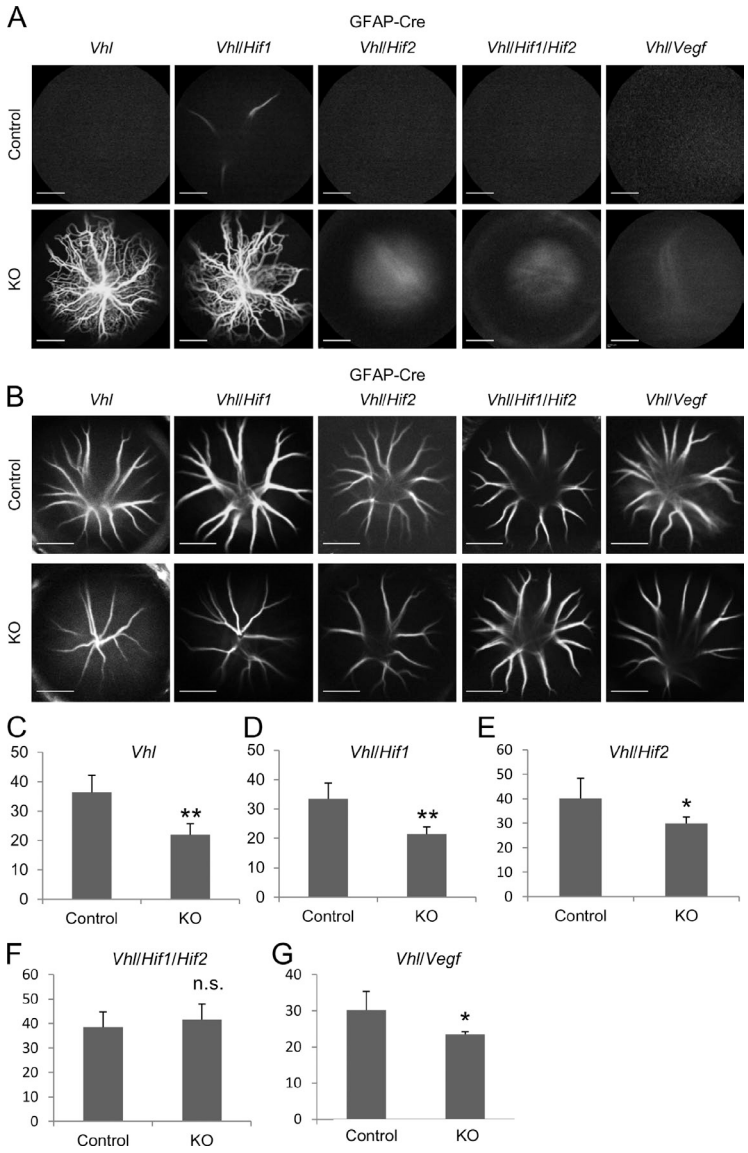

Figure 3. **Secondary outgrowth but not accelerated hyaloidal regression in Vhl mutants is caused via the HIF-2/VEGF signaling pathway.** (A) Secondary outgrowth in various combinations of astrocyte-specific knockout (KO) mice at P40. Note that massive secondary outgrowth is observed in *Vhl* (both HIF-1α and HIF-2α are stabilized) and *Vhl/Hif-1α* double mutants (only HIF-2α is stabilized). The outgrowth phenotype is prevented in *Vhl/Hif-2α* (only HIF-1α is stabilized), in *Vhl/Hif-1α/Hif-2α*, or in *Vhl/Vegf* mutants, demonstrating that HIF-2α/VEGF signaling is required for the development of secondary outgrowth. (B–G) Representative hyaloidal vascular images (B) and numbers of branching points (C–G) in various combinations of knockout mice at P14 (n = 4–8). Note that accelerated hyaloidal regression is observed in *Vhl* (C), *Vhl/Hif-1α* (D), *VHL/Hif-2α* (E), *and Vhl/Vegf* (G) but not *Vhl/Hif-1α/Hif-2α* (F) mutants, demonstrating that HIF-1α and HIF-2α compensate for this phenotype independently from VEGF. n.s., not significant. *, P < 0.05; **, P < 0.01. Error bars indicate mean ± SD. Bars, 2,000 µm.

Similar changes were observed in *Vhl* mutants (P = 0.00035 and 0.00044 for *Mif* and *F4/80*, respectively; Fig. S5 A) but not in *Vhl/Hif-1α* double mutants (Fig. S5 B). These data suggest that constitutively active HIF-1α may activate *Mif* up-regulation in *Vhl* mutants and induce infiltration of circulating macrophages, leading to accelerated hyaloidal regression. This is significant because others have shown that macrophages have clear functions in hyaloidal vessel regression (Lang and Bishop, 1993; Lobov et al., 2005), but the manner in which they are recruited is not clear.

To identify the molecular activities of HIF-1α in astrocytes, we performed overexpression assays in the murine C8-D1A astrocyte line. These cells exhibit fibrous astrocytic morphologies and express GFAP (Alliot and Pessac, 1984). Using immunohistochemistry, we detected robust levels of MIF in the cytoplasm of these cells (costaining with phalloidin and DAPI mark the contours and nuclei of the cells; Fig. 4 D). Constitutively active *Hif-1α* (*CA–Hif-1α*) or *Hif-2α* (*CA–Hif-2α*) expression constructs were used; these constructs were generated using site-directed mutagenesis to remove the pVHL-binding sequences (P402A/P564A and P405A/P531A, respectively; Yan et al., 2007). C8-D1A cells were cotransfected with *Gfp* to monitor transfection efficiency, and *Hif-1α* and *Hif-2α* overexpression was confirmed using RT-PCR (Fig. 4 E). The effects of transfecting *CA–Hif-1α* and *CA–Hif-2α* in vitro were monitored using RT-PCR and quantitative sandwich ELISAs. *Vegf*, a well-established target of HIFs, is significantly up-regulated after *CA–Hif-2α* transfection (P = 0.00024; Fig. 4 E). Increases in secreted VEGF protein were also observed (2.42-fold; P = 0.009; Fig. 4 F). These data are compatible with previous findings showing that HIF-2α (but not HIF-1α) in astrocytes is responsible for regulating VEGF or erythropoietin production in vivo during hypoxia or after *Vhl* deletion (Weidemann et al., 2009, 2010). Surprisingly, the transfection of *CA–Hif-1α* induces significant *Mif* up-regulation (P = 0.00057; Fig. 4 E) and 10.1-fold (P = 0.008) secreted protein production (Fig. 4 F); no difference in *Mif* mRNA and MIF protein induction by *CA–Hif-2α* is observed in *Gfp*-transfected controls (Fig. 4, E and F). There have been no previous reports of a gene being predominantly regulated by HIF-1α in astrocytes.

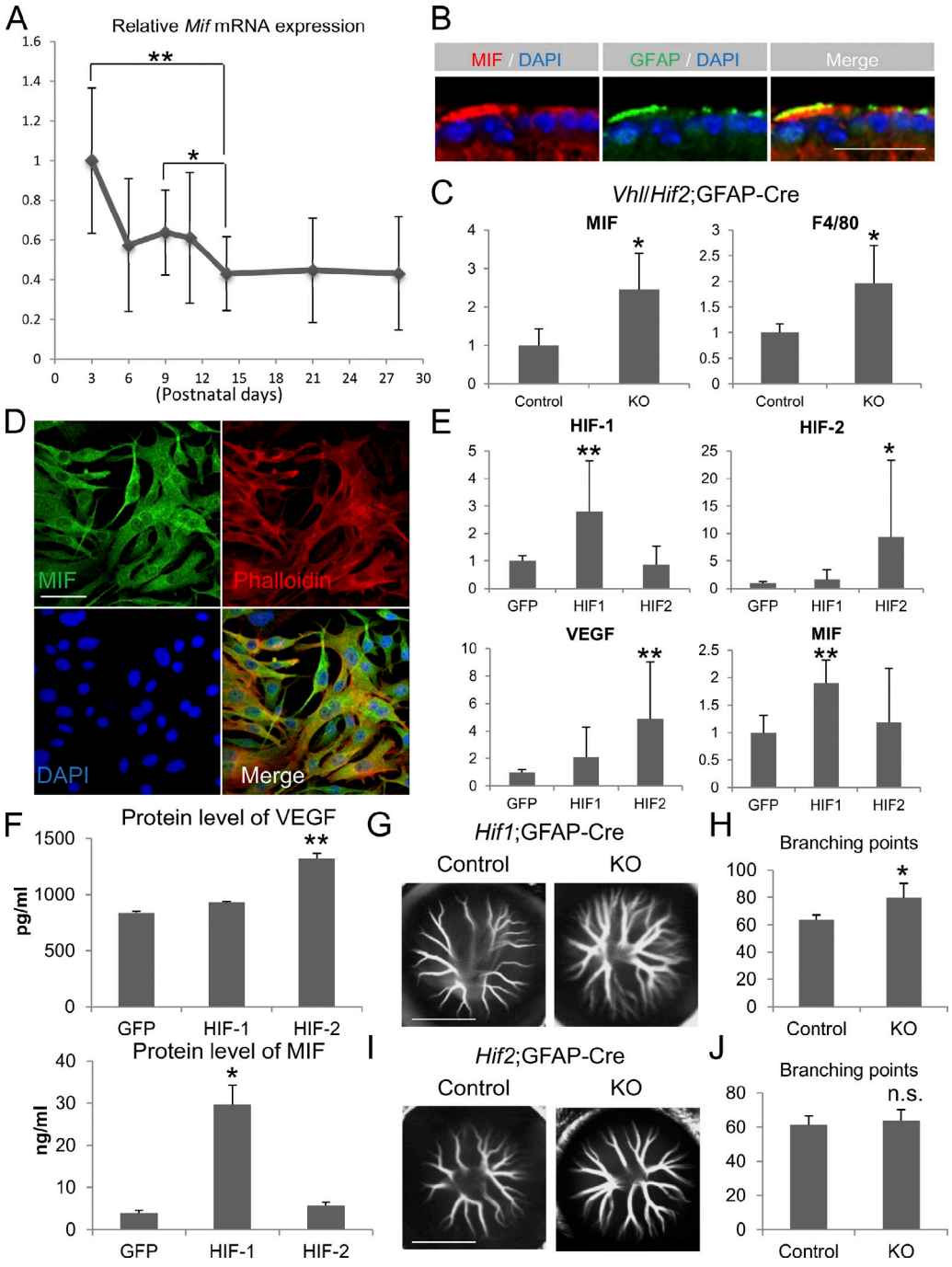

Figure 4. **HIF-1α, but not HIF-2α, regulates MIF in astrocytes.** (A) *Mif* mRNA expression was monitored by real-time RT-PCR and plotted on a scatter plot at P3, 6, 9, 11, 14, 21, and 28 early postnatal stages of hyaloidal vessel regression in isolated retinas. Note that significant down-regulation is observed at P14 compared with P3 (n = 8). (B) Immunohistochemistry with MIF and GFAP antibodies in P14 retinal ganglion cell layer is shown. Note that MIF expression is colocalized with astrocytes in the ganglion cell layer. (C) *Mif* and *F4/80* mRNA expression in *Vhl/Hif-2α* double mutants at P14. Note that the ectopic stabilization of HIF-1α in retinal astrocytes results in simultaneous (and significant) up-regulation of *Mif* and *F4/80* (n = 4). KO, knockout. (D) Immunocytochemistry for MIF was performed on cultured C8-D1A murine astrocyte cells. Note that MIF is robustly expressed in the cytoplasm (visualized with phalloidin labeling) of C8-D1A cells (all cells are counterstained with DAPI). (E) Relative mRNA expression of *Hif-1α*, *Hif-2α*, *Vegf*, and *Mif* in C8-D1A cells transfected with *CA–Hif-1α*, *CA–Hif-2α*, or *Gfp*. Note that the transfection of *CA–Hif-1α* induces *Hif-1α* in C8-D1A (top left), and *CA–Hif-2α* induces robust *Hif-2α* expression (top right). *Vegf* is up-regulated significantly (4.9-fold; P = 0.00024) when C8-D1A cells are transfected with *CA–Hif-2α*. *Mif* is significantly (1.9-fold; P = 0.000057) up-regulated by *CA–Hif-1α* (n = 11–12). (F) VEGF and MIF-secreted protein levels were measured from supernatants of *CA–Hif-1α* or *CA–Hif-2α*–transfected C8-D1A cells using quantitative sandwich ELISAs (n = 5–6). VEGF secretion is significantly (2.7-fold; P = 0.009) up-regulated by *CA–Hif-2α* (top). MIF is significantly (7.6-fold; P = 0.03) up-regulated by *CA–Hif-1α* (bottom). (G–J) Representative hyaloidal vasculature (G and I) and number of branching points (H and J) in HIF-1α (G and H) or HIF-2α (I and J) mutants are shown at P9 (n = 6). Note that in HIF-1α mutants, delayed hyaloidal regression compared with control littermate is observed in early postnatal stages. n.s., not significant. *, P < 0.05; **, P < 0.01. Error bars indicate mean ± SD. Bars: (B) 20 μm; (D) 50 μm; (G and I) 2,000 μm.

To investigate the function of HIF-1α in physiological hyaloidal regression, we quantified the numbers of branching points of the hyaloidal vasculature in astrocyte-specific *Hif-1α* or *Hif-2α* mutants at an early postnatal stage (P9) when *Mif* is expressed at significantly higher levels compared with a later stage, P14 (Fig. 4 A). In *Hif-1α* mutants, hyaloidal regression was delayed significantly compared with control littermates (P = 0.036; Fig. 4 G; quantified in Fig. 4 H), and no significant difference was observed in *Hif-2α* mutants and controls (Fig. 4, I and J). In later stages (P14) when *Mif* was normally down-regulated (Fig. 4 A), no difference was observed between *Hif-1α* or *Hif-2α* mutants and controls (Fig. S5, C–F). These data confirm that HIF-1α is required for physiological hyaloidal regression and for regulating *Mif* expression in astrocytes during hypoxic early postnatal stages.

The intravitreal injection of recombinant MIF or astrocytes transfected with *CA–Hif-1α* accelerates hyaloidal vessel regression

To determine whether HIF-1α/MIF signaling is sufficient to accelerate hyaloidal vessel regression, we examined the contribution of each factor in vivo using overexpression and hyperactivation assays. We assessed the role of astrocytes overexpressing HIF-1α by transplanting C8-D1A cells transfected with *CA–Hif-1α/Gfp* or *Gfp* alone. After transfection in vitro, adherent cells were released from temperature-sensitive UpCell matrices (thus preserving their surface antigens) and injected intravitreally into P11 mouse eyes. To monitor the transplanted GFP-transfected astrocytes, we used CSLO (Fig. 5 A). 3 d after injection with *CA–Hif-1α/Gfp* (or only *Gfp*)–transfected C8-D1A cells, the hyaloidal vasculature was examined in vivo using ICG angiography (Fig. 5, B and C). We observed a significant reduction in the number of branching points (P = 0.0020; Fig. 5 C) in eyes injected with *CA–Hif-1α/Gfp* compared with those injected with *Gfp* alone. We also injected equal numbers of *CA–Hif-1α*–transfected cells (no *Gfp*) and untransfected cells as controls in eyes of *CX3CR1*$^{GFP/+}$ transgenic mice in which myeloid cells are genetically labeled with GFP (Jung et al., 2000). Using CSLO, we observed a dramatic increase in the number of infiltrating GFP-positive macrophages in eyes injected with *CA–Hif-1α*–transfected astrocytes compared with controls (Fig. 5 D). Furthermore, RT-PCR analyses with F4/80 probes performed in lysates from retinas injected with *CA–Hif-1α*–transfected astrocytes reveal a significant up-regulation (P = 0.049; Fig. 5 E). There is a concomitant increase in the number of recruited macrophages, which may explain how hyaloidal vessel regression was accelerated in *Vhl* mutants.

To determine whether MIF alone is sufficient to promote macrophage infiltration and hyaloidal vessel regression, we injected recombinant murine MIF (rmMIF) into wild-type mouse eyes. We observed a dose-dependent, significant reduction of hyaloidal vascular branching points in rmMIF-injected eyes compared with vehicle-injected eyes (P = 0.060 and 0.00042 for 1,000 and 100 ng of rmMIF, respectively; Fig. 5 F; quantified in Fig. 5 G). Furthermore, the injection of recombinant rmMIF also induced GFP-positive cell infiltration in *CX3CR1*$^{GFP/+}$ mice (Fig. 5 H) and up-regulation of *F4/80* (P = 0.016; Fig. 5 I), demonstrating that, like *Hif-1α*, MIF is sufficient to induce macrophage-mediated vascular remodeling in the eye. Finally, we also treated a set of mice with three i.p. injections of a specific MIF antagonist, ISO-1 (35 mg/kg), or vehicle over 6 d starting at P8. This dosage has been shown to be effective in blocking lipopolysaccharide-induced sepsis in mice (Al-Abed et al., 2005). In mice treated with ISO-1, significantly more branching points were observed than in vehicle-injected mice, suggesting that endogenous MIF regulates normal hyaloidal regression (P = 0.012; Fig. 5 J; quantified in Fig. 5 K). In another set of mice, ISO-1 was injected three times, 3 d and 1 d before and 1 d after intravitreal astrocyte injection. No significant differences were observed between groups pretreated with ISO-1 and then injected with *CA–Hif-1α/GFP* or *GFP*-transfected control astrocytes (P = 0.39; Fig. 5 L; quantified in Fig. 5 M), demonstrating that the MIF antagonist effectively neutralizes the *CA–Hif-1α/GFP*–mediated accelerated regression. These findings support the concept that HIF-1α/MIF signaling is necessary and sufficient to recruit circulating macrophages into the vitreous and regulate hyaloidal vessel regression.

Macrophage-derived MIF also acts to accelerate hyaloidal regression in an autocrine manner

Having established a role for the astrocyte-specific pVHL/HIF-1/MIF pathway in the regulation of hyaloidal vascular growth and regression, we also investigated the role of this pathway in macrophages using conditional gene inactivation. pVHL was deleted in myeloid cell lineages (including macrophages) using *M lysozyme* (*LysM*)–*Cre* mice (Clausen et al., 1999). In this line, significantly accelerated hyaloidal regression also was observed compared with control littermates (P = 0.0032; Fig. 6, A and B). RT-PCR analyses performed on the retinas of these mice revealed up-regulation of *Mif* and *F4/80* (P = 0.015 and 0.037, respectively; Fig. 6 C), suggesting that even increases in autocrine-delivered MIF from macrophages themselves can promote the recruitment of additional migratory macrophages from the general circulation and accelerate the rate of hyaloidal vessel regression. Additionally, the conditional deletion of endogenous *Vegf* in myeloid cells does not induce any appreciable alteration of the rate of hyaloidal vessel regression (Fig. S5, G and H). Consequently, alterations to oxygen concentration in the eye may induce both astrocytes and macrophages to secrete MIF, which then recruits macrophages into the eye and regulates vascular remodeling.

Discussion

In this study, we used combinatorial conditional gain- and loss-of-function assays to reveal that pVHL in astrocytes is necessary and sufficient for hyaloidal vessel regression. When *Vhl* is deleted, we observe two primary phenotypes: accelerated primary hyaloidal vascular regression and massive secondary outgrowth of hyaloidal vessels (Fig. 2). Our combinatorial genetic deletion strategies clearly demonstrate that VHL/HIF-2α/VEGF signaling is responsible for inducing the

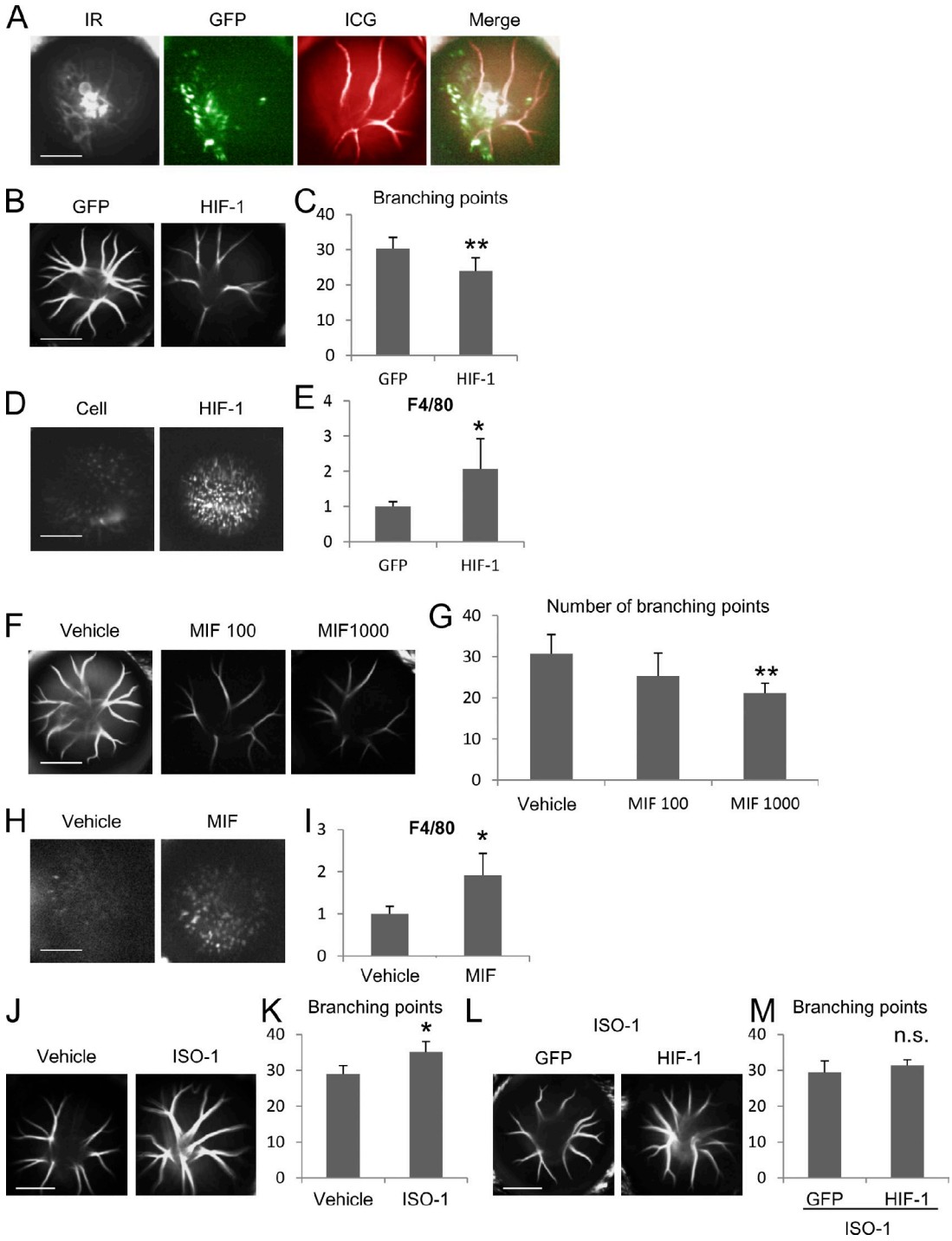

Figure 5. **HIF-1α/MIF signaling in astrocytes is sufficient in vivo to regulate macrophage accumulation and hyaloidal vessel regression.** (A) *Gfp*-transfected C8-D1A cells (green) were transplanted into the vitreous space and visualized with ICG-infused hyaloidal vasculature (red) by CSLO in vivo. IR, infrared images (white). (B and C) Representative hyaloidal vascular images (B) and numbers of branching points (C) at P14 3 d after transplantation of *Gfp* or *CA–Hif-1α/Gfp*–transfected C8-D1A cells (n = 6–11). Note that the numbers of hyaloidal vessels are significantly reduced in eyes injected with *CA–Hif-1α/Gfp*–transfected C8-D1A cells compared with *Gfp* only–transfected cells. (D) Representative images of GFP fluorescence from myeloid cells in *CX3CR1*$^{GFP/+}$ mice 3 d after transplantation of untransfected or *Hif-1α*–transfected C8-D1A cells. Note that increased macrophage accumulation after transplantation of *Hif-1α*–transfected cells is confirmed in the transgenic mice. (E) Relative *F4/80* mRNA expression detected by real-time RT-PCR (n = 4). Significant up-regulation of *F4/80* was observed in retinal/vitreal lysates after transplantation with *CA–Hif-1α/Gfp*–transfected astrocytes compared with *Gfp*-transfected controls. (F and G) Representative hyaloidal vascular images (F) and numbers of branching points (G) at P14 3 d after injection of rmMIF. Note that injection of rmMIF induces accelerated hyaloidal regression significantly (1,000 ng of rmMIF; MIF 1000) compared with PBS (vehicle)-injected eyes. (H) Representative images of GFP signaling in *CX3CR1*$^{GFP/+}$ mice 3 d after 1,000 ng of rmMIF. (I) Real-time RT-PCR detected significant up-regulation of *F4/80* with MIF injection compared with vehicle (n = 4). (J–M) Representative hyaloidal vascular images (J and L) and numbers of branching points (K and M) at P14 after i.p. injection of an MIF inhibitor, ISO-1, at P8, 10, and 12 with (L and M) or without (J and K) transplantation of *Gfp* or *CA–Hif-1α/Gfp*–transfected C8-D1A cells at P11 (n = 4–6). Note that injection of ISO-1 slows the rate of hyaloidal vessel regression significantly (K). Pretreating mice with ISO-1 rescues the accelerated regression phenotype induced by injecting *CA–Hif-1α*–transfected astrocytes at the same stage (M). n.s., not significant. *, $P < 0.05$; **, $P < 0.01$. Error bars indicate mean ± SD. Bars, 2,000 µm.

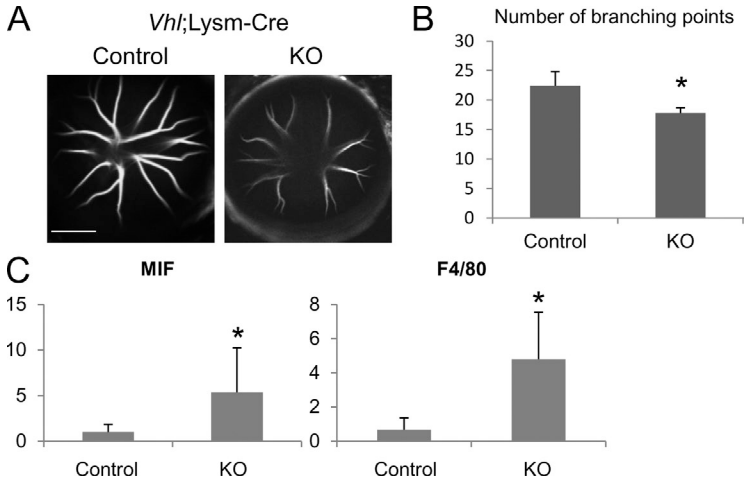

Figure 6. **Myeloid cell–specific *Vhl* deletion induces accelerated hyaloidal vascular regression.** (A and B) Representative images of hyaloidal vasculature (A) and numbers of branching points (B) in myeloid cell–specific *Vhl;Lysm-Cre* mutant mice (n = 4–6). Note that significantly accelerated hyaloidal regression was observed in macrophage *Vhl* mutants at P16. KO, knockout. Bar, 2,000 µm. (C) Quantitative RT-PCR for *Mif* and *F4/80* in macrophage *Vhl* mutants (n = 4). Note that *Mif* and *F4/80* are significantly upregulated in mutants compared with controls, suggesting that autocrine MIF secretion from macrophages causes tissue infiltration of macrophages that mediate the accelerated regression. *, $P < 0.05$. Error bars indicate mean ± SD.

secondary hyaloidal outgrowth (Fig. 3). Previous studies have shown that although HIF-1α is expressed in astrocytes, its function was unknown (Weidemann et al., 2009, 2010). In this study, we observe that HIF-1α in astrocytes functions to regulate hyaloidal vascular regression by inducing the production of MIF, which leads to the recruitment of macrophages critical to the vascular remodeling associated with the shift in the retina from embryonic to adult vasculature (Figs. 4 and 5). Finally, we demonstrate that both paracrine- and autocrine-derived MIF is required to regulate hyaloidal regression (Fig. 6). From these observations, we conclude that careful regulation of divergent HIF-1α and HIF-2α functions is critical, as ectopic stabilization leads to significant ocular vascular abnormalities (Fig. 7).

We demonstrate a previously unreported role for HIF-1α in vascular remodeling: regulating MIF expression and macrophage infiltration in vivo. Although not all cells express both HIF-1α and HIF-2α, in those that do (i.e., epidermal cells, hepatocytes, intestinal epithelium cells, and astrocytes), HIF-2α tends to function in a dominant manner (Rankin et al., 2007, 2008; Boutin et al., 2008; Mastrogiannaki et al., 2009; Weidemann et al., 2009). Although HIF-2α alone does mediate accelerated regression in *Vhl* mutants through an unknown mechanism that merits future study (Fig. 3 D), we do show that HIF-1α has an important role not only during abnormal accelerated regression but also during physiological regression (Fig. 4, G and H). These observations, describing differential and essential roles of HIF-1α and HIF-2α in astrocytes, reveal a novel mechanism of pathological vascular remodeling.

In utero, physiological hypoxia is required for normal development in various tissues. Previous studies (Chen et al., 2008; Kurihara et al., 2010), as well as this study, have shown that changes in oxygen availability may drive pVHL-dependent degradation of HIF-αs and initiate ablation and clearance of the fetal vasculature. In humans, growth of the retinal vascular network and regression of the hyaloidal vessels start in the third trimester. An oxygen-sensing role for astrocytes has been proposed in the central nervous system (Bernaudin et al., 2000) and may exhibit a similar role in the retina, where these cells can also influence the developing retinal vasculature (West et al., 2005). The data presented in this study support these models and strongly suggest that failure of oxygen sensing in astrocytes induces a PHPV-like picture as a result of an imbalance of the divergent functions of HIF-1α and HIF-2α. This may explain why the hyaloidal vessels regress at distinct time points in humans and rodents (the third trimester in utero and early postnatal stages, respectively), as hyaloidal vascular regression occurs simultaneously with development of the retinal vascular networks in both systems.

Vhl mutants share several ocular phenotypic characteristics with human PHPV (Reese, 1955; Goldberg, 1997). Human PHPV is clinically classified according to three types—anterior, posterior, and mixed—based on where the persistent vessels are observed. The massive secondary outgrowth (commonly referred to as a retrolental mass characteristic of anterior PHPV) extends from the central stalk (characteristic of posterior PHPV). Thus, the vascular network of the secondary outgrowth observed in *Vhl* mutants is typical of human mixed PHPV (Fig. 2). Other transgenic mouse models (i.e., mutations to *p19^{Arf}*, *Norrin*, *Fz4*, and *Angiopoietin-2*) also share some features of PHPV (Hackett et al., 2002; McKeller et al., 2002; Xu et al., 2004). However, defective retinal vascularization is also observed in some of these models, suggesting that the persistent hyaloidal vessels may be preserved to compensate for retinal hypo- or avascularity. In contrast, astrocyte *Vhl* mutant mice have highly vascularized retinas (Fig. S3) and, thus, more closely resemble that observed in human PHPV. Although the density of astrocytes is also increased in *Vhl* mutants (Fig. S4), we argue that this phenomenon alone cannot induce the PHPV-like phenotype. Data from multiple in vivo and in vitro assays more strongly suggest that the phenotype is induced by intrinsically modulating the HIF-1/MIF and HIF-2/VEGF pathways (Figs. 3–5). The progression of human PHPV is difficult to monitor, as it occurs in utero but currently is widely accepted to be a failure of hyaloidal vessel regression. Surprisingly and importantly, the current model presented in this study suggests that PHPV in humans may not be caused by incomplete primary regression but rather aberrant secondary angiogenesis, as revealed using novel in vivo vascular monitoring techniques and daily observations (Fig. 2).

The observations made in our study may have applications for understanding the mechanisms involved in replacing

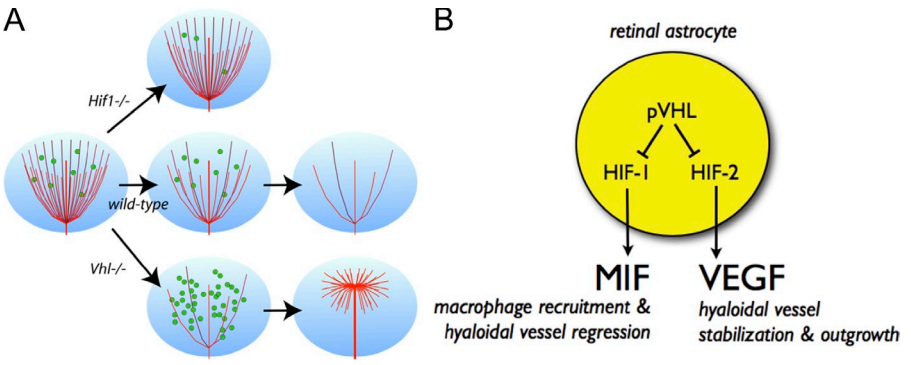

Figure 7. **Current hypothetical model for pVHL-controlled hyaloidal vascular remodeling.** (A) Hyaloidal vasculature regression is directed by the oxygen-sensing pVHL/HIF pathway in astrocytes to regulate the flux of infiltrating macrophages. In *Hif-1α* mutants, *Mif* levels are attenuated, fewer macrophages are recruited into the vitreous, and hyaloidal vasculature regression is retarded. In *Vhl* mutants, MIF levels increase dramatically as a result of HIF-1α stabilization; this results in accelerated hyaloidal vasculature regression. Increases in VEGF secretion as a result of HIF-2α stabilization stabilize the stalk of the hyaloidal network and induce secondary outgrowth of vessels along a superficial plane. (B) Astrocytes sense fluctuations in oxygen concentrations in the retina and respond by suppressing pVHL. This in turn stabilizes HIF-1α and HIF-2α that regulate MIF and VEGF, respectively. HIF-1α/MIF signaling regulates macrophage recruitment and controls the rate of hyaloidal vessel regression. Conversely, HIF-2α/VEGF signaling induces pathological neovascularization of hyaloidal vessels when dysregulated.

embryonic with adult vasculature in other tissues (i.e., cardiac, pulmonary, or umbilical systems). Macrophage recruitment by MIF may promote key remodeling events to initiate vascular remodeling and regeneration of diseased tissues. It may also be possible to use recombinant MIF as a tool to modulate tumor vasculature. Furthermore, therapies targeting HIF-1α and HIF-2α in astrocytes or macrophages using specific antagonists may also prove to be effective modulators of pathological angiogenesis in multiple tissues.

Materials and methods

Mice

All procedures involving animals were approved by the Scripps Research Institute Animal Care Committee, which ensures that all federal guidelines concerning animal experimentation are met. Transgenic mice expressing Cre recombinase under *GFAP* (*GFAP-Cre* mice; Bajenaru et al., 2002) or *LysM* promoter (*LysM-Cre* mice; Clausen et al., 1999) were mated with $Vhl^{floxed/floxed}$ (Haase et al., 2001), $Hif\text{-}1\alpha^{floxed/floxed}$ (Ryan et al., 2000), or $Hif\text{-}2\alpha^{floxed/floxed}$ (Gruber et al., 2007) or $Vegf^{floxed/floxed}$ mice (Gerber et al., 1999). As control littermates, floxed mice without Cre transgene were used. To monitor Cre recombination in *GFAP-Cre* mice in astrocytes, we mated them with ROSA26 (reverse orientation splice acceptor 26) mTomato/mGFP transgenic reporter mice (Muzumdar et al., 2007). To monitor myeloid cells in vivo, $CX3CR1^{GFP/+}$ mice (Jung et al., 2000) were used.

Vascular corrosion casting

Plastic resin was prepared using a vasQtec kit according to the manufacturer's instructions. Green fluorescent pigment (vasQtec) was added to the resin to improve visualization for imaging. Mice were slowly perfused using published protocols with a cerebral spinal fluid–like solution followed by 2% formalin (Sigma-Aldrich) in PBS and then followed by the resin (Krucker et al., 2006). After the perfusion, the plastic hardened for at least 5 d before the soft tissues were dissolved with 7.5% KOH (Sigma-Aldrich) at 50°C overnight. The casts were decalcified in 2.5% formic acid (Sigma-Aldrich) for 12 h at 50°C. The casts were imaged in PBS at room temperature on an upright confocal microscope (LSM 510; Carl Zeiss) with a 5× objective lens (EC Plan-Neofluar 5×/0.16; Carl Zeiss). 3D reconstructions were generated using ZEN 2010 software (Carl Zeiss).

In vivo hyaloidal vasculature imaging

To monitor hyaloidal regression in vivo, we used CSLO (SPECTRALIS; Heidelberg Engineering). Mice were anesthetized by an i.p. injection of 15 mg/kg ketamine and 7 mg/kg xylazine, and ICG (50 µg/g body weight) was injected intraperitoneally. Pupils were dilated immediately before imaging with 1% tropicamide and 2.5% phenylephrine. To quantify the numbers of the branching points, images were obtained by five different angles from each animal. Branching points were manually counted. The branching points in the central vasculature were counted first, and then the peripheral branches were counted. Peripheral branching points were only counted when they did not appear in the center image (Fig. S1).

Immunofluorescence

Whole-mount preparations were performed as previously described (Weidemann et al., 2010). In brief, retinae were fixed in 4% PFA for 1 h. After blocking with 10% FBS (Invitrogen) and 10% normal goat serum (The Jackson Laboratory) in PBS for 1 h, retinae were incubated with the primary antibodies described below, washed, and incubated with the fluorescence-conjugated secondary antibody (1:200 dilution; Invitrogen). Retinae were then laid flat with four radial relaxing incisions and mounted for whole-mount image capturing using confocal microscopy. For immunohistochemistry, eyes were enucleated after euthanasia, fixed in ice-cold 4% PFA (Electron Microscopy Sciences), and embedded in OCT compound (Sakura). For immunocytochemistry, cells grown in chambered slides (Lab-Tek II; Nalge Nunc International) were briefly fixed in room temperature 4% PFA. Tissues and cells were briefly permeabilized with 1.0 or 0.5% Triton X-100 (Sigma-Aldrich), respectively, before blocking with 2% normal goat serum solution (Jackson ImmunoResearch Laboratories, Inc.). 2-h room temperature incubations were performed with all primary antibodies. After washing with PBS, secondary antibodies (Alexa Fluor 488, 568 or 594, and 647; Invitrogen) diluted 1:1,000 were added for 30 min. Cells were counterstained with DAPI (Invitrogen) and washed before mounting. The following primary antibodies were used in this study: chicken polyclonal GFAP (1:2,000; Abcam), rabbit polyclonal GFAP (1:1,000; Invitrogen), rabbit polyclonal MIF (1:50; Santa Cruz Biotechnology, Inc.), rabbit polyclonal GFP (1:100; Abcam), and fluorescent-conjugated phalloidin (1:2,000). Fluorescent-conjugated isolectin *Griffonia Simplicifolia IB-4* was also used (GS-lectin; Invitrogen). Imaging was performed in a mounting medium (SlowFade gold antifade reagent; Invitrogen) at room temperature on a confocal microscope (LSM 710; Carl Zeiss) with an EC Plan-Neofluar 10×/0.30, Plan-Apochromat 20×/0.80, or Plan-Apochromat 40×/0.95 objective lens (Carl Zeiss). All images are processed with ZEN 2010 software.

RT-PCR analysis

Total RNA was prepared from vitreo-retinal tissues using the RNeasy Plus Mini kit (QIAGEN) and was reverse transcribed using Superscript II (Invitrogen). Quantitative PCR assays were performed on a real-time PCR System (ABI 7900HT Fast) using a PCR master mix (TaqMan Fast Universal; Applied Biosystems) and TaqMan gene expression assay mix of *hif-1a* (Mm00468869_m1), *hif-2a* (Mm00438717_m1), *vegfa* (Mm00437304_m1), *mif* (Mm01611157_gH), and *f4/80* (Mm00802530_m1). Eukaryotic 18S ribosomal RNA TaqMan minor groove binder probe was used as an endogenous control. Data were analyzed with 7900HT Fast System SDS software (version 2.4; Applied Biosystems). All experiments were performed with four replicates.

ELISA

We measured murine MIF and murine VEGF expression levels using colorimetric quantitative sandwich ELISA kits (R&D Systems or Kamiya Biomedical Company, respectively). 2 d after transfection, 2 mL of media was removed from cells grown in 6-well plates and concentrated using centrifugal filters (Amicon Ultra 10K; Millipore). Each condition was tested in triplicate according to the manufacturer's specifications, and the output was measured using a microplate reader (Synergy 2; BioTek). Concentrations were obtained by fitting the data to a standard curve using nonlinear four-factor regression.

Tissue culture

The mouse astrocyte C8-D1A line was obtained from American Type Culture Collection. Cells were maintained at 37° and 5% CO_2 in DME with GlutaMax (Invitrogen) and 10% FBS (Invitrogen). C8-D1A cells were transfected using Attractene (QIAGEN) using a total DNA/Attractene ratio of 0.6 µg/1.5 µl using a fast-forward protocol and plated on UpCell 6-well plates (Thermo Fisher Scientific). Media was replaced after 6 h to stop the reaction. Transfections were confirmed by monitoring GFP fluorescence. DNA constructs for *HA–HIF-1α P402A/P564A* (*CA–Hif-1α*) and *HA–Hif-2α P405A/P531A* (*CA–Hif-2α*) were deposited by W.G. Kaelin (plasmids 18955 and 18956; Addgene; Yan et al., 2007). pMaxGFP (Lonza) was cotransfected to label transfected cells in some experiments.

Astrocyte injections

Transfected C8-D1A astrocytes were collected from UpCell plates by replacing the media with room temperature PBS and incubating the plate at room temperature until the cells were released. In this way, all surface proteins remained intact before transplantation. Roughly 250,000 transfected or untransfected control cells in 50 µl were injected in each P11 mouse eye (intravitreal). In other eyes, either 1.0 or 0.1 µg of recombinant carrier-free MIF reconstituted in PBS (R&D Systems) was injected again in 50 µl volumes. At least six eyes were injected for each experimental condition. 2 d after transfecting C8-D1A cells with *CA–Hif-1α/Gfp*, *CA–Hif-2α/Gfp*, or *Gfp* alone, the cells were released from the UpCell plates. 3 d later, the hyaloidal vasculature was examined in vivo using ICG angiography.

Statistical analysis

Comparison between the mean variables of two groups was performed by a two-tailed Student's *t* test. $P < 0.05$ was considered to be statistically significant.

Online supplemental material

Fig. S1 shows the quantification method for hyaloidal vascular branching points. Fig. S2 shows that hyaloidal vasculature does not contain GFAP-positive cells. Fig. S3 characterizes Cre-mediated recombination in astrocytes of GFAP-Cre mice. Fig. S4 shows retinal vasculature of *Vhl;GFAP-Cre* mice. Fig. S5 provides additional characterization of mRNA expression and hyaloidal vasculature in various mutant mice. Online supplemental material is available at http://www.jcb.org/cgi/content/full/jcb.201107029/DC1.

We would like to thank Alison L. Dorsey, Melissa S. Henrie, Keeley Shaw, and Mollie S. Friedlander for the excellent technical assistance.

This work was supported by grants to M. Friedlander from the National Eye Institute (EY-11254) and the Lowy Medical Research Foundation. T. Kurihara is supported by a fellowship from the Manpei Suzuki Diabetes Foundation and The Japan Society for the Promotion of Science Postdoctoral Fellowships for Research Abroad. P.D. Westenskow is a Ruth L. Kirschstein Fellow of the National Institutes of Health (EY021416).

Submitted: 6 July 2011
Accepted: 17 October 2011

References

Al-Abed, Y., D. Dabideen, B. Aljabari, A. Valster, D. Messmer, M. Ochani, M. Tanovic, K. Ochani, M. Bacher, F. Nicoletti, et al. 2005. ISO-1 binding to the tautomerase active site of MIF inhibits its pro-inflammatory activity and increases survival in severe sepsis. *J. Biol. Chem.* 280:36541–36544. http://dx.doi.org/10.1074/jbc.C500243200

Albè, E., J.H. Chang, N.F. Azar, A.R. Ivanov, and D.T. Azar. 2008. Proteomic analysis of the hyaloid vascular system regression during ocular development. *J. Proteome Res.* 7:4904–4913. http://dx.doi.org/10.1021/pr800551m

Alliot, F., and B. Pessac. 1984. Astrocytic cell clones derived from established cultures of 8-day postnatal mouse cerebella. *Brain Res.* 306:283–291. http://dx.doi.org/10.1016/0006-8993(84)90377-9

Bajenaru, M.L., Y. Zhu, N.M. Hedrick, J. Donahoe, L.F. Parada, and D.H. Gutmann. 2002. Astrocyte-specific inactivation of the neurofibromatosis 1 gene (NF1) is insufficient for astrocytoma formation. *Mol. Cell. Biol.* 22:5100–5113. http://dx.doi.org/10.1128/MCB.22.14.5100-5113.2002

Bernaudin, M., A. Bellail, H.H. Marti, A. Yvon, D. Vivien, I. Duchatelle, E.T. Mackenzie, and E. Petit. 2000. Neurons and astrocytes express EPO mRNA: Oxygen-sensing mechanisms that involve the redox-state of the brain. *Glia.* 30:271–278. http://dx.doi.org/10.1002/(SICI)1098-1136(200005)30:3<271::AID-GLIA6>3.0.CO;2-H

Bloom, B.R., and B. Bennett. 1966. Mechanism of a reaction in vitro associated with delayed-type hypersensitivity. *Science*. 153:80–82. http://dx.doi.org/10.1126/science.153.3731.80

Boutin, A.T., A. Weidemann, Z. Fu, L. Mesropian, K. Gradin, C. Jamora, M. Wiesener, K.U. Eckardt, C.J. Koch, L.G. Ellies, et al. 2008. Epidermal sensing of oxygen is essential for systemic hypoxic response. *Cell*. 133:223–234. http://dx.doi.org/10.1016/j.cell.2008.02.038

Brown, A.S., L. Leamen, V. Cucevic, and F.S. Foster. 2005. Quantitation of hemodynamic function during developmental vascular regression in the mouse eye. *Invest. Ophthalmol. Vis. Sci.* 46:2231–2237. http://dx.doi.org/10.1167/iovs.04-0848

Chen, Y., Y.Q. Doughman, S. Gu, A. Jarrell, S. Aota, A. Cvekl, M. Watanabe, S.L. Dunwoodie, R.S. Johnson, V. van Heyningen, et al. 2008. Cited2 is required for the proper formation of the hyaloid vasculature and for lens morphogenesis. *Development*. 135:2939–2948. http://dx.doi.org/10.1242/dev.021097

Clausen, B.E., C. Burkhardt, W. Reith, R. Renkawitz, and I. Förster. 1999. Conditional gene targeting in macrophages and granulocytes using LysMcre mice. *Transgenic Res.* 8:265–277. http://dx.doi.org/10.1023/A:1008942828960

Diez-Roux, G., and R.A. Lang. 1997. Macrophages induce apoptosis in normal cells in vivo. *Development*. 124:3633–3638.

Gerber, H.P., K.J. Hillan, A.M. Ryan, J. Kowalski, G.A. Keller, L. Rangell, B.D. Wright, F. Radtke, M. Aguet, and N. Ferrara. 1999. VEGF is required for growth and survival in neonatal mice. *Development*. 126:1149–1159.

Goldberg, M.F. 1997. Persistent fetal vasculature (PFV): An integrated interpretation of signs and symptoms associated with persistent hyperplastic primary vitreous (PHPV). LIV Edward Jackson Memorial Lecture. *Am. J. Ophthalmol.* 124:587–626.

Gruber, M., C.J. Hu, R.S. Johnson, E.J. Brown, B. Keith, and M.C. Simon. 2007. Acute postnatal ablation of Hif-2alpha results in anemia. *Proc. Natl. Acad. Sci. USA*. 104:2301–2306. http://dx.doi.org/10.1073/pnas.0608382104

Haase, V.H., J.N. Glickman, M. Socolovsky, and R. Jaenisch. 2001. Vascular tumors in livers with targeted inactivation of the von Hippel-Lindau tumor suppressor. *Proc. Natl. Acad. Sci. USA*. 98:1583–1588. http://dx.doi.org/10.1073/pnas.98.4.1583

Hackett, S.F., S. Wiegand, G. Yancopoulos, and P.A. Campochiaro. 2002. Angiopoietin-2 plays an important role in retinal angiogenesis. *J. Cell. Physiol.* 192:182–187. http://dx.doi.org/10.1002/jcp.10128

Ito, M., and M. Yoshioka. 1999. Regression of the hyaloid vessels and pupillary membrane of the mouse. *Anat. Embryol. (Berl.)*. 200:403–411. http://dx.doi.org/10.1007/s004290050289

Jung, S., J. Aliberti, P. Graemmel, M.J. Sunshine, G.W. Kreutzberg, A. Sher, and D.R. Littman. 2000. Analysis of fractalkine receptor CX(3)CR1 function by targeted deletion and green fluorescent protein reporter gene insertion. *Mol. Cell. Biol.* 20:4106–4114. http://dx.doi.org/10.1128/MCB.20.11.4106-4114.2000

Kato, M., M.S. Patel, R. Levasseur, I. Lobov, B.H. Chang, D.A. Glass II, C. Hartmann, L. Li, T.H. Hwang, C.F. Brayton, et al. 2002. *Cbfa1*-independent decrease in osteoblast proliferation, osteopenia, and persistent embryonic eye vascularization in mice deficient in Lrp5, a Wnt coreceptor. *J. Cell Biol.* 157:303–314. http://dx.doi.org/10.1083/jcb.200201089

Krucker, T., A. Lang, and E.P. Meyer. 2006. New polyurethane-based material for vascular corrosion casting with improved physical and imaging characteristics. *Microsc. Res. Tech.* 69:138–147. http://dx.doi.org/10.1002/jemt.20263

Kurihara, T., Y. Kubota, Y. Ozawa, K. Takubo, K. Noda, M.C. Simon, R.S. Johnson, M. Suematsu, K. Tsubota, S. Ishida, et al. 2010. von Hippel-Lindau protein regulates transition from the fetal to the adult circulatory system in retina. *Development*. 137:1563–1571. http://dx.doi.org/10.1242/dev.049015

Lang, R., M. Lustig, F. Francois, M. Sellinger, and H. Plesken. 1994. Apoptosis during macrophage-dependent ocular tissue remodelling. *Development*. 120:3395–3403.

Lang, R.A., and J.M. Bishop. 1993. Macrophages are required for cell death and tissue remodeling in the developing mouse eye. *Cell*. 74:453–462. http://dx.doi.org/10.1016/0092-8674(93)80047-I

Lobov, I.B., S. Rao, T.J. Carroll, J.E. Vallance, M. Ito, J.K. Ondr, S. Kurup, D.A. Glass, M.S. Patel, W. Shu, et al. 2005. WNT7b mediates macrophage-induced programmed cell death in patterning of the vasculature. *Nature*. 437:417–421. http://dx.doi.org/10.1038/nature03928

Lutty, G.A., D.C. Thompson, J.Y. Gallup, R.J. Mello, A. Patz, and A. Fenselau. 1983. Vitreous: An inhibitor of retinal extract-induced neovascularization. *Invest. Ophthalmol. Vis. Sci.* 24:52–56.

Mastrogiannaki, M., P. Matak, B. Keith, M.C. Simon, S. Vaulont, and C. Peyssonnaux. 2009. HIF-2alpha, but not HIF-1alpha, promotes iron absorption in mice. *J. Clin. Invest.* 119:1159–1166. http://dx.doi.org/10.1172/JCI38499

Maxwell, P.H., M.S. Wiesener, G.W. Chang, S.C. Clifford, E.C. Vaux, M.E. Cockman, C.C. Wykoff, C.W. Pugh, E.R. Maher, and P.J. Ratcliffe. 1999. The tumour suppressor protein VHL targets hypoxia-inducible factors for oxygen-dependent proteolysis. *Nature*. 399:271–275. http://dx.doi.org/10.1038/20459

McKeller, R.N., J.L. Fowler, J.J. Cunningham, N. Warner, R.J. Smeyne, F. Zindy, and S.X. Skapek. 2002. The Arf tumor suppressor gene promotes hyaloid vascular regression during mouse eye development. *Proc. Natl. Acad. Sci. USA*. 99:3848–3853. http://dx.doi.org/10.1073/pnas.052484199

Meeson, A., M. Palmer, M. Calfon, and R. Lang. 1996. A relationship between apoptosis and flow during programmed capillary regression is revealed by vital analysis. *Development*. 122:3929–3938.

Messmer-Blust, A., X. An, and J. Li. 2009. Hypoxia-regulated angiogenic inhibitors. *Trends Cardiovasc. Med.* 19:252–256. http://dx.doi.org/10.1016/j.tcm.2010.02.006

Muzumdar, M.D., B. Tasic, K. Miyamichi, L. Li, and L. Luo. 2007. A global double-fluorescent Cre reporter mouse. *Genesis*. 45:593–605. http://dx.doi.org/10.1002/dvg.20335

Preis, I., R. Langer, H. Brem, and J. Folkman. 1977. Inhibition of neovascularization by an extract derived from vitreous. *Am. J. Ophthalmol.* 84:323–328.

Rankin, E.B., M.P. Biju, Q. Liu, T.L. Unger, J. Rha, R.S. Johnson, M.C. Simon, B. Keith, and V.H. Haase. 2007. Hypoxia-inducible factor-2 (HIF-2) regulates hepatic erythropoietin in vivo. *J. Clin. Invest.* 117:1068–1077. http://dx.doi.org/10.1172/JCI30117

Rankin, E.B., J. Rha, T.L. Unger, C.H. Wu, H.P. Shutt, R.S. Johnson, M.C. Simon, B. Keith, and V.H. Haase. 2008. Hypoxia-inducible factor-2 regulates vascular tumorigenesis in mice. *Oncogene*. 27:5354–5358. http://dx.doi.org/10.1038/onc.2008.160

Reese, A.B. 1955. Persistent hyperplastic primary vitreous. *Trans. Am. Acad. Ophthalmol. Otolaryngol.* 59:271–295.

Ryan, H.E., M. Poloni, W. McNulty, D. Elson, M. Gassmann, J.M. Arbeit, and R.S. Johnson. 2000. Hypoxia-inducible factor-1alpha is a positive factor in solid tumor growth. *Cancer Res.* 60:4010–4015.

Weidemann, A., Y.M. Kerdiles, K.X. Knaup, C.A. Rafie, A.T. Boutin, C. Stockmann, N. Takeda, M. Scadeng, A.Y. Shih, V.H. Haase, et al. 2009. The glial cell response is an essential component of hypoxia-induced erythropoiesis in mice. *J. Clin. Invest.* 119:3373–3383.

Weidemann, A., T.U. Krohne, E. Aguilar, T. Kurihara, N. Takeda, M.I. Dorrell, M.C. Simon, V.H. Haase, M. Friedlander, and R.S. Johnson. 2010. Astrocyte hypoxic response is essential for pathological but not developmental angiogenesis of the retina. *Glia*. 58:1177–1185.

Welford, S.M., B. Bedogni, K. Gradin, L. Poellinger, M. Broome Powell, and A.J. Giaccia. 2006. HIF1alpha delays premature senescence through the activation of MIF. *Genes Dev.* 20:3366–3371. http://dx.doi.org/10.1101/gad.1471106

West, H., W.D. Richardson, and M. Fruttiger. 2005. Stabilization of the retinal vascular network by reciprocal feedback between blood vessels and astrocytes. *Development*. 132:1855–1862. http://dx.doi.org/10.1242/dev.01732

Xu, Q., Y. Wang, A. Dabdoub, P.M. Smallwood, J. Williams, C. Woods, M.W. Kelley, L. Jiang, W. Tasman, K. Zhang, and J. Nathans. 2004. Vascular development in the retina and inner ear: Control by Norrin and Frizzled-4, a high-affinity ligand-receptor pair. *Cell*. 116:883–895. http://dx.doi.org/10.1016/S0092-8674(04)00216-8

Yan, Q., S. Bartz, M. Mao, L. Li, and W.G. Kaelin Jr. 2007. The hypoxia-inducible factor 2alpha N-terminal and C-terminal transactivation domains cooperate to promote renal tumorigenesis in vivo. *Mol. Cell. Biol.* 27:2092–2102. http://dx.doi.org/10.1128/MCB.01514-06

Ye, X., Y. Wang, H. Cahill, M. Yu, T.C. Badea, P.M. Smallwood, N.S. Peachey, and J. Nathans. 2009. Norrin, frizzled-4, and Lrp5 signaling in endothelial cells controls a genetic program for retinal vascularization. *Cell*. 139:285–298. http://dx.doi.org/10.1016/j.cell.2009.07.047

Yu, D.Y., and S.J. Cringle. 2001. Oxygen distribution and consumption within the retina in vascularised and avascular retinas and in animal models of retinal disease. *Prog. Retin. Eye Res.* 20:175–208. http://dx.doi.org/10.1016/S1350-9462(00)00027-6